PIER C

(Received 6 September 2025, Accepted 7 October 2025, Scheduled 17 October 2025)

A Deadbeat Predictive Disturbance Suppression Model for Permanent Magnet Synchronous Motor Flux Weakening Control

Han Liu, Yang Yu, Xin Wang*, Zhixin Liu, and Zehua Gong

School of Electrical Information Engineering, Jiangsu University of Technology, Changzhou 213001, China

ABSTRACT: To enhance the robustness and dynamic performance of permanent magnet synchronous motor (PMSM) drives at high speeds, a deadbeat predictive current control method based on a predictive disturbance suppression model (DPCC-PDSM) is proposed. First, the mathematical model of PMSM and the principle of traditional deadbeat predictive current control (DPCC) are presented. Second, to estimate and compensate disturbance effects caused by external uncertainties, a predictive disturbance suppression model is designed by integrating the recursive least squares (RLS) algorithm with an extended state observer (ESO). Furthermore, leading angle flux weakening control strategy is incorporated into the predictive control framework to overcome voltage and current limitations in high-speed operation. Finally, the stability and effectiveness of the proposed method are validated through experiments. The results demonstrate that the DPCC-PDSM significantly improves robustness and ensures the stable and reliable performance of PMSM drives in high-speed flux weakening operation.

1. INTRODUCTION

With the advent of modern computer numerical control (CNC) machine tools, high-speed machining capability has become a key performance indicator. To ensure superior dynamic response and control precision under high-speed operation, many CNC systems now employ permanent magnet synchronous motors (PMSMs) as spindle drives. With their high efficiency, rapid response, and precise control [1, 2], PMSMs are well suited for high-end CNC applications requiring frequent start-stop and stringent dynamic performance. However, as spindle speeds rise, conventional control strategies face voltage and current limitations, which degrade stability and speed regulation in high-speed regions — becoming a bottleneck for further performance improvement.

To overcome these challenges, advanced control strategies have been proposed. Among them, model predictive control (MPC) has gained attention for handling system constraints while ensuring excellent dynamics [3–5]. Deadbeat predictive current control, a representative MPC strategy, determines optimal voltage vectors in real time to achieve fast current dynamics and negligible steady-state error [6]. Yet, deadbeat predictive current control (DPCC) remains sensitive to parameter mismatches and disturbances. To enhance robustness, extended state observers (ESOs) have been incorporated, modeling disturbances as augmented states for effective suppression [7–9].

Data-driven approaches further improve PMSM robustness. Deep reinforcement learning and adaptive control have optimized DPCC, enhancing adaptability and dynamics [10–12]. Oversampling DPCC with field programmable gate array (FPGA) technology enables constant switching frequency and reduced current ripple [13]. Sliding mode control-based DPCC boosts anti-disturbance ability [14–16], while dynamic time-planning-based dead beat control for six-phase PMSM addresses multi-objective optimization under fault scenarios [17–19]. Still, robustness under parameter uncertainties remains limited. To address this, a DPCC algorithm based on a predictive disturbance suppression model is proposed, where prediction errors are introduced as compensation to strengthen robustness.

Meanwhile, flux weakening (FW) control has been widely adopted to overcome voltage limits and extend PMSM speed range. In CNC machining, FW allows spindle motors to sustain acceleration in the constant power region. For example, an enhanced FW scheme with polar-coordinate computation ensures smooth transitions, torque integration, and improved voltage utilization [20–22]. In five-phase PMSM, harmonic current injection with feedforward FW and gradient descent reduces distortion under DPCC [23]. For asymmetric rotor PMSM, an improved leading angle flux weakening control dynamically adjusts current vector angles to enable wide-speed operation [24]. Prior research also shows that FW modules enhance torque and speed response under varying loads [25]. To improve tracking in FW regions, indirect coupling models (ICMs) have been proposed [26, 27].

For asymmetric PMSM, reoriented d-axis reference frames correct voltage-limit distortions and support deep FW [28–32]. However, current regulators risk saturation and instability in deep FW regions, threatening stability and safety. Ensur-

* Corresponding author: Xin Wang (wx_simba@jsut.edu.cn).

ing smooth, stable transitions during high-speed FW operation therefore remains a central challenge for PMSM drives.

In response to the above issues, this paper proposes a high-speed spindle control strategy for CNC machines that integrates a predictive disturbance suppression model with leading angle flux weakening control. The proposed approach leverages PDSM to enhance robustness against external disturbances, while leading angle flux weakening control alleviates voltage constraints in deep flux weakening regions. Experimental validation demonstrates that the proposed method significantly improves current regulation stability and high-speed control performance, while substantially reducing dynamic response time.

2. DEADBEAT AND FLUX WEAKENING CONTROL

2.1. Mathematical Modeling of PMSM and DPCC Principle

The two-phase stator voltage equations of PMSM are:

$$\begin{cases} u_d = Ri_d + L_d\dfrac{di_d}{dt} - L_q\omega_e i_q, \\ u_q = Ri_q + L_q\dfrac{di_q}{dt} + L_d\omega_e i_d + \omega_e\psi_f. \end{cases} \tag{1}$$

where u_d and u_q are the stator voltage components in the d-axis and q-axis; i_d and i_q are the stator current components in the d-axis and q-axis; R is the stator resistance; L_d and L_q are the stator inductances in the d-axis and q-axis, respectively; and ψ_f is the permanent magnet flux linkage.

In order for the PMSM model to be implemented in digital control systems, we need to discretize these continuous equations. Assuming that we use the first-order Taylor expansion to discretize the time derivative, the derivative of the current can be approximated by the first-order difference:

$$\begin{cases} \dfrac{di_d}{dt} \approx \dfrac{i_d(k+1) - i_d(k)}{T_s} \\ \dfrac{di_q}{dt} \approx \dfrac{i_q(k+1) - i_q(k)}{T_s} \end{cases} \tag{2}$$

where $i_d(k+1)$ and $i_q(k+1)$ denote the d-axis and q-axis current components at the $(k+1)^{\text{th}}$ sampling instant, respectively; $i_d(k)$ and $i_q(k)$ denote the corresponding components at the k^{th} instant; and T_s is the sampling interval. By substituting the first-order difference expressions in (2) into the original stator voltage equations, we obtain:

$$\begin{cases} u_{d(k)} = L\left(\dfrac{i_d(k+1) - i_d(k)}{T_s}\right) + Ri_d(k) \\ \qquad - \omega_e L i_q(k) \\ u_{q(k)} = L\left(\dfrac{i_q(k+1) - i_q(k)}{T_s}\right) + Ri_q(k) \\ \qquad + \omega_e L i_d(k) + \omega_e\psi_f \end{cases} \tag{3}$$

where $u_{d(k)}$ and $u_{q(k)}$ are the d-axis and q-axis stator voltage components at sampling instant k, respectively; R is the stator resistance; L is the inductance; ω_e is the electrical angular velocity at time k; and ψ_f is the permanent magnet flux linkage.

The surface-mounted permanent magnet synchronous motor (SPMSM) is considered, with the d- and q-axis inductances assumed equal, i.e., $L_d = L_q = L$. The unified symbol L is then used in Equations (3) and (4) for simplicity.

The principle of Deadbeat Predictive Current Control is to use a predictive model to estimate the motor current at the next time step, and then compute the required stator voltage to achieve zero steady-state error in current tracking. Under the control strategy where $i_d = 0$, the reference currents $i_d^*(k+1)$ and $i_q^*(k+1)$ are used as predicted current values at the next sampling instant T_{k+1}, replacing the actual currents $i_d(k+1)$ and $i_q(k+1)$ in the prediction model. By substituting these reference currents into Equation (3), the predictive model for the deadbeat current control can be expressed as:

$$\begin{cases} u_{d(k)} = L\left(\dfrac{i_d^*(k) - i_d(k)}{T_s}\right) + Ri_d(k) \\ \qquad - \omega_e L i_q(k) \\ u_{q(k)} = L\left(\dfrac{i_q^*(k) - i_q(k)}{T_s}\right) + Ri_q(k) \\ \qquad + \omega_e L i_d(k) + \omega_e\psi_f \end{cases} \tag{4}$$

where $i_d^*(k)$ and $i_q^*(k)$ represent the d-axis and q-axis current components at time step $k+1$, respectively. They indicate the expected current state of the motor in the next control cycle.

2.2. Flux Weakening Control and Limiting Conditions

Flux weakening control is widely applied to extend the speed range of PMSMs beyond their rated limits. By injecting a negative d-axis current, the stator-generated magnetic field is intentionally reduced, which lowers the air-gap flux linkage and back electromotive force (EMF), enabling stable high-speed operation.

As rotor speed increases, the back EMF may approach or exceed the DC bus voltage, limiting further acceleration under standard control. Flux weakening control offsets this effect by suppressing the EMF rise, thereby allowing reliable high-speed performance and maintaining system stability.

In flux weakening mode, the relationship between motor speed and stator voltage can be expressed as:

$$\omega_e = \frac{u_s}{\sqrt{(L_q i_q)^2 + (L_d i_d + T_s\psi_f)^2}} \tag{5}$$

where u_s is the magnitude of the stator voltage vector, defined as $u_s = \sqrt{u_d^2 + u_q^2}$, while i_d and i_q are the corresponding components of the stator current; L_d and L_q are the d- and q-axis inductances; ψ_f is the permanent magnet flux linkage; and T_s is the sampling period.

When the motor reaches its voltage limit, further speed increase requires adjusting the stator current distribution. This is

typically done by increasing the negative d-axis current and reducing the q-axis current. It weakens the air-gap flux, allowing the motor to operate at higher speeds through flux weakening control.

In a PMSM control system, operation is constrained by two main factors: the rated current of the motor and the DC bus voltage of the inverter. The control strategy must ensure that both current and voltage stay within limits, which are defined as follows:

$$\begin{cases} u_d^2 + u_q^2 \le U_{\max}^2 \\ i_d^2 + i_q^2 \le I_{\max}^2 \end{cases} \tag{6}$$

where $U_{\max}$ is the voltage limit, and $I_{\max}$ is the current limit. The voltage limit $U_{\max}$ is typically chosen as $U_{\mathrm{dc}}/\sqrt{3}$. As shown in Fig. 1, these inequalities define the voltage and current limit boundaries for the permanent magnet synchronous motor.

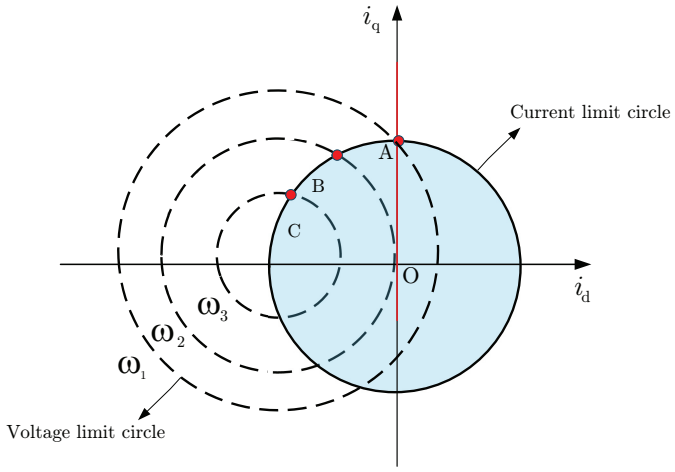

FIGURE 1. Current and voltage limiting circle.

3. PREDICTIVE DISTURBANCE SUPPRESSION MODEL AND LEADING ANGLE FLUX WEAKENING CONTROL

3.1. Observer Design Based on ESO

Traditional deadbeat control generally achieves high precision compared with PI control. However, if a sudden change in motor parameters or a significant external disturbance occurs during control, the traditional deadbeat control may exhibit undesirable behavior. To mitigate the influence of external disturbances on the system, we introduce an ESO. This observer estimates the predictive current error in real time to provide compensation and guides the design of the predictive disturbance suppression model. The observer is designed as follows:

$$\begin{cases} \mathbf{u}^* = L\left(\dfrac{i^* - i}{T_s}\right) + Ri - L\omega_e i + \hat{\eta} + L \cdot G_1 \Delta i(k) \\ \dot{\hat{\eta}} = G_2 \Delta i(k) \end{cases} \tag{7}$$

where u^* denotes the predicted control voltage vector generated by the observer for disturbance compensation; $\hat{\eta}$ is the estimated disturbance state variable; $\Delta i(k)$ is the predicted current error; and G_1 and G_2 are gain coefficients.

3.2. Design of Predictive Disturbance Suppression Model

Introducing an ESO can suppress external disturbances. However, due to parameter mismatches, the disturbance often exhibits strong nonlinear characteristics, making it impractical to obtain an accurate mathematical model of the disturbance directly.

To address this issue, this paper employs Recursive Least Squares algorithm to fit the disturbance, resulting in a new predictive disturbance suppression model. The model is designed as follows:

$$\begin{cases} \hat{\eta}_{d(k+1)} = \hat{\eta}_{d(k)} + G_2 K\left(\Delta i_d(k)\right) T_s \\ \hat{\eta}_{q(k+1)} = \hat{\eta}_{q(k)} + G_2 K\left(\Delta i_q(k)\right) T_s \end{cases} \tag{8}$$

where $\hat{\eta}_d(k)$ and $\hat{\eta}_q(k)$ are the estimated disturbance states along the d- and q-axes at time k, and $\hat{\eta}_d(k+1)$ and $\hat{\eta}_q(k+1)$ are the corresponding predicted disturbance states at time $k+1$. $K(\Delta i_d(k))$ and $K(\Delta i_q(k))$ are the prediction current errors, while G_1 and G_2 are gain coefficients. The framework is illustrated in Fig. 2.

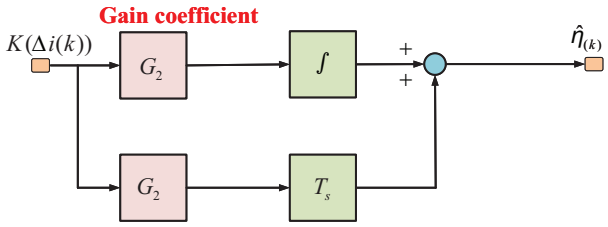

FIGURE 2. Estimate disturbance state variable frame diagram.

By substituting Equation (8) into Equation (4), we obtain:

$$\begin{cases} u_d^* = L\left(\dfrac{i_d^*(k) - i_d(k)}{T_s}\right) + Ri_d(k) - L\omega_e i_q(k) \\ \qquad + \hat{\eta}(k) + LG_1 K(\Delta i_d(k)) \\ u_q^* = L\left(\dfrac{i_q^*(k) - i_q(k)}{T_s}\right) + Ri_q(k) + L\omega_e i_d(k) \\ \qquad + \omega_e \psi_{f0} + \hat{\eta}(k) + LG_1 K(\Delta i_q(k)) \end{cases} \tag{9}$$

where u_d^* and u_q^* are the predicted control voltages along the d- and q-axes, respectively; $i_d^*(k)$ and $i_q^*(k)$ are the reference currents at the k-th sampling instant; $i_d(k)$ and $i_q(k)$ are the actual currents; $\hat{\eta}(k)$ represents the estimated disturbance; and L, R, ω_e, and ψ_{f0} are the system parameters. Here, we reiterate that this study focuses on SPMSM, where $L_d = L_q = L$, and therefore a unified inductance L is consistently adopted in Equation (9). The predicted current error $\Delta i(k)$ is calculated using the Recursive Least Squares method as follows:

$$\begin{cases} K(\Delta i_d(k)) = E \cdot \Delta i_d(k) \\ K(\Delta i_q(k)) = E \cdot \Delta i_q(k) \end{cases} \tag{10}$$

During each sampling period, the current error $\Delta \mathbf{i}(k)$ is computed and updated using the least-squares error coefficient matrix $\mathbf{C}(k)$. This predicted current error is then applied to update the estimated motor parameters $\mathbf{w}(k)$.

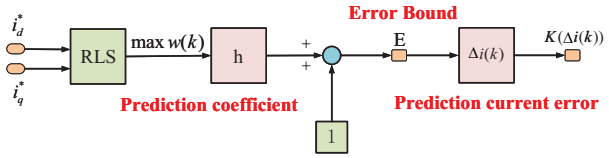

FIGURE 3. RLS fitting of PDSM.

To ensure system stability and performance, the algorithm also tracks the maximum observed values of the motor parameters throughout operation. As illustrated in Figure 3, the RLS algorithm continuously refines the parameter estimates by adjusting the error coefficient matrix $\mathbf{C}(k)$ in response to real-time variations, thereby improving the accuracy of the motor model. The detailed computation procedure is described as follows.

First, we define the state vector as:

$$\mathbf{v}(k) = \begin{bmatrix} 1 \\ k \end{bmatrix} \tag{11}$$

where k denotes the sample index, representing the discrete time step. The state vector $\mathbf{v}(k)$ serves as the input signal for the Recursive Least Squares algorithm.

Next, the current error $\Delta\mathbf{i}(k)$, representing the deviation between the reference and actual current values, is calculated as:

$$\begin{cases} \Delta i_d(k) = i_d^*(k) - i_d(k) \\ \Delta i_q(k) = i_q^*(k) - i_q(k) \end{cases} \tag{12}$$

To facilitate the RLS update, the absolute value of the current error is taken to form the scalar measurement value $y(k)$:

$$y(k) = |\Delta\mathbf{i}(k)| \tag{13}$$

Following this, the covariance matrix $\mathbf{C}(k)$ is updated based on the standard RLS recursive formulation:

$$\mathbf{C}(k) = \mathbf{C}(k-1) - \frac{\mathbf{C}(k-1)\mathbf{v}(k)\mathbf{v}(k)^T\mathbf{C}(k-1)^T}{1 + \mathbf{v}(k)^T\mathbf{C}(k-1)\mathbf{v}(k)} \tag{14}$$

where $\mathbf{C}(k)$ is the covariance matrix at time step k; $\mathbf{C}(k-1)$ represents the covariance matrix from the previous time step; and $\mathbf{v}(k)$ is the state vector at time step k.

Next, we calculate prediction error $\delta(k)$. Prediction error represents the difference between the actual output $y(k)$ and predicted output based on the parameters $\mathbf{w}(k-1)$ at the previous time step. The calculation formula is:

$$\delta(k) = y(k) - \mathbf{v}^T(k)\mathbf{w}(k-1) \tag{15}$$

where $\mathbf{v}^T(k)\mathbf{w}(k-1)$ is the output of the parameter estimation $\mathbf{w}(k-1)$ and the state vector $\mathbf{v}(k)$ at the previous time step. Based on gain matrix $\mathbf{C}(k)$ and prediction error $\delta(k)$, we update the calculation of motor parameters. The update formula is:

$$\mathbf{w}(k) = \mathbf{w}(k-1) + \mathbf{C}(k)\mathbf{v}(k)\delta(k) \tag{16}$$

where $\mathbf{C}(k)$ is the updated gain matrix, and $\mathbf{v}(k)$ is the state vector at the current time, while $\delta(k)$ is the prediction error.

To track the maximum estimation parameters, we need to check whether the previous estimated parameter exceeds the maximum value and update the maximum value:

$$\max \mathbf{w}(k) = \max(\mathbf{w}(k), \max(\mathbf{w}(k))) \tag{17}$$

The proposed observer is a dynamic adaptive observer that can execute both forward prediction and primary prediction. To avoid system oscillation and instability, parameter E is limited as follows:

$$E = \max(\mathbf{w}(k)) + h \tag{18}$$

3.3. Leading Angle Flux Weakening Control

The traditional flux weakening control usually uses a fixed current vector distribution to achieve speed regulation. However, at high speeds, it is easily affected by voltage limits and current saturation, making it difficult to maintain output performance. Although the output can be adjusted by changing the ratio of the direct-axis current to the quadrature-axis current, this method cannot fully utilize the voltage capability of the inverter at high speeds, which limits system performance.

Therefore, the advanced leading angle flux weakening control strategy is introduced. By adjusting the phase angle of the current vector, the magnetic field is effectively weakened, thereby improving the stability and speed regulation ability of the motor at high speed.

This method achieves flux weakening expansion by controlling the phase angle (β) of the current vector. The mathematical formulation is expressed as follows:

$$\begin{cases} i_d = I_s \cdot \cos\beta \\ i_q = I_s \cdot \sin\beta \end{cases} \tag{19}$$

To optimize motor performance at high speeds, the leading angle flux weakening control adjusts the phase angle of the current vector to enhance the utilization of the terminal voltage relative to the DC bus voltage.

When the motor speed exceeds its rated value, this method increases the leading angle β of the current vector through a proportional-integral (PI) regulator. In this way, the direct-axis current component i_d is increased while the quadrature-axis current component i_q is reduced. As a result, the back electromotive force is weakened, allowing the motor to operate stably under high-speed conditions, as illustrated in Fig. 4.

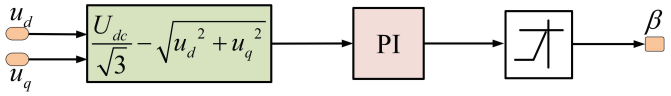

FIGURE 4. The leading angle of current vector in flux weakening control.

As shown in Fig. 5, the optimization is achieved by regulating the proportion of current components. The system controls the current vector and phase angle β of the motor using a proportional-integral regulator. The PI controller continuously eliminates the steady-state speed error and generates the corresponding control signal. To ensure stability, phase angle β is further constrained within the range of 0 to $-\pi/2$, which prevents excessive modulation and guarantees reliable high-speed operation.

By dynamically computing and updating the phase angle β in real time, the system adaptively adjusts both the direct-axis

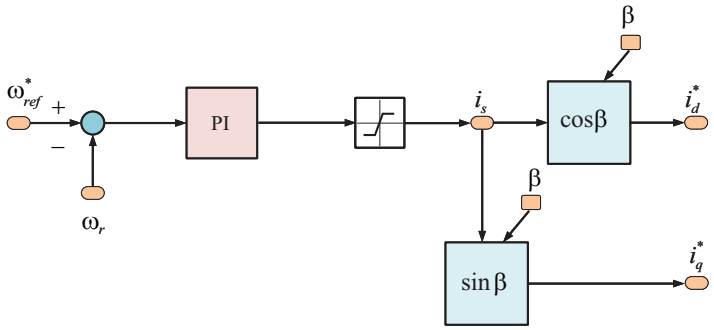

FIGURE 5. Leading angle flux weakening control.

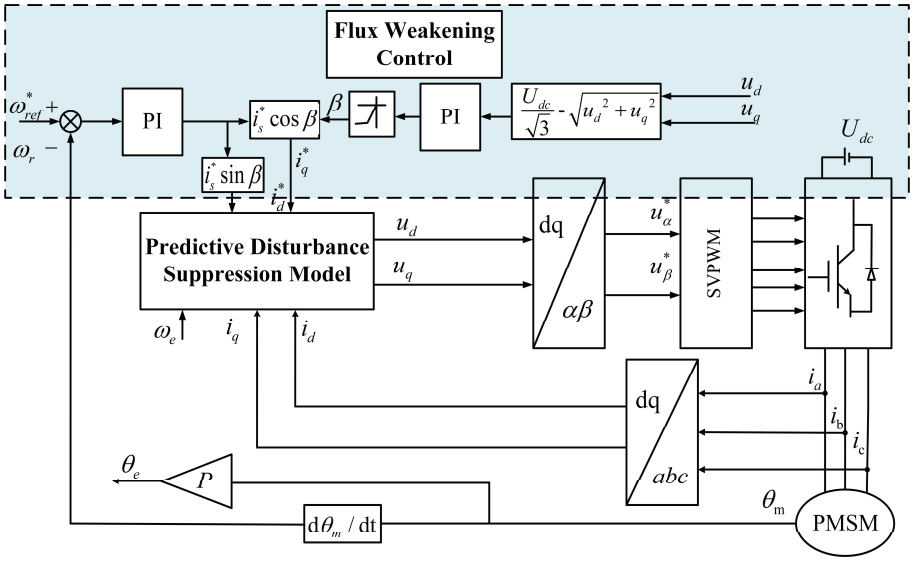

FIGURE 6. Permanent magnet synchronous motor deadbeat flux weakening control overall frame diagram.

(i_d) and quadrature-axis (i_q) current components. This coordinated regulation reduces the effective back electromotive force, enhances the flux-weakening capability at elevated speeds, and significantly improves the efficiency of high-speed regulation. As a result, the motor is able to sustain stable operation under demanding conditions, extend its operating speed range beyond the rated limit, and achieve improved reliability and control precision.

An improved PMSM control framework is proposed by combining the predictive disturbance suppression model and leading angle flux weakening control strategy, as shown in Fig. 6. The framework consists of two core modules.

Firstly, the PDSM module addresses problems caused by external disturbances. The recursive least squares algorithm and ESO are used to predict and compensate disturbances in real time, thereby enhancing robustness and stability, ensuring effective disturbance suppression at high speeds, and maintaining precise motor control.

Secondly, the leading angle flux weakening control module optimizes the motor's magnetic field by adjusting phase angle β of the current vector. This approach overcomes the voltage and current limitations of traditional control methods in the high-speed region and improves the speed-regulation performance of the motor.

In addition, PI controller is employed to accurately regulate the direct-axis current i_d and quadrature-axis current i_q, ensuring both dynamic response and stable operation of the motor under varying conditions. By integrating disturbance prediction and current regulation, the overall control strategy effectively enhances performance and reliability of the motor in high-speed and complex environments.

4. EXPERIMENT

As shown in Fig. 7, the PMSM used in the experiment has the following key technical parameters: DC bus voltage $U_{\mathrm{dc}} = 310\,\mathrm{V}$, rated speed 6000 r/min, pole pairs $p = 4$, stator resistance $R = 1.6\,\Omega$, stator inductance $L = 5.075\,\mathrm{mH}$, and rotor flux linkage $\psi_f = 0.0825\,\mathrm{Wb}$. Some of the main rated parameters, such as rated power, rated current, rated voltage, and rated torque, are listed in Table 1. In addition, the control hardware adopts a digital signal processor (DSP) (TMS320F28335) and current sensors (ACS712, 20 A), which ensures accurate measurement and reproducibility. Regarding the control strategy, the experiment applies vector control with $i_d = 0$, and the torque is regulated by i_q.

In this experiment, under weak flux weakening conditions with a target speed of 6000 r/min, which corresponds to the

TABLE 1. Parameters of the PMSM.

Parameters	Value	Parameters	Value
Rated power (P_r)	0.2 kW	Rated current (I_s)	2.1 A
Stator resistance (R_s)	1.6 Ω	Permanent magnet flux linkage (ψ_f)	0.08Wb
Inductance (L_s)	5.07mH	Pole pairs	4
Rated voltage (U_{dc})	310 V	Rated torque (T_e)	0.64 N · m

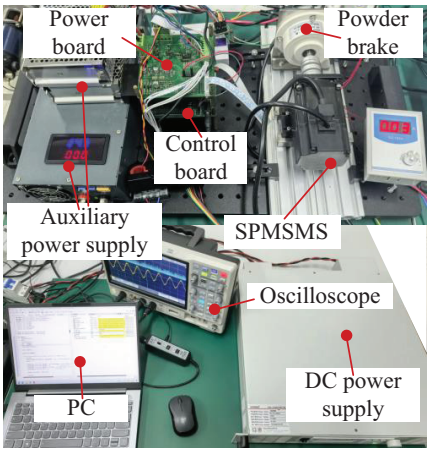

FIGURE 7. PMSM experimental platform.

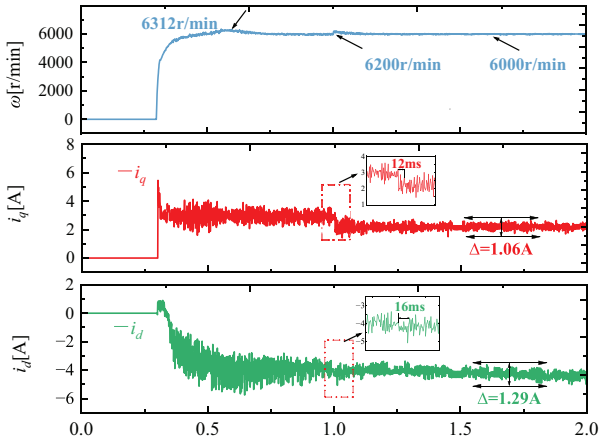

FIGURE 8. Speed and current response under PI control with load step disturbance.

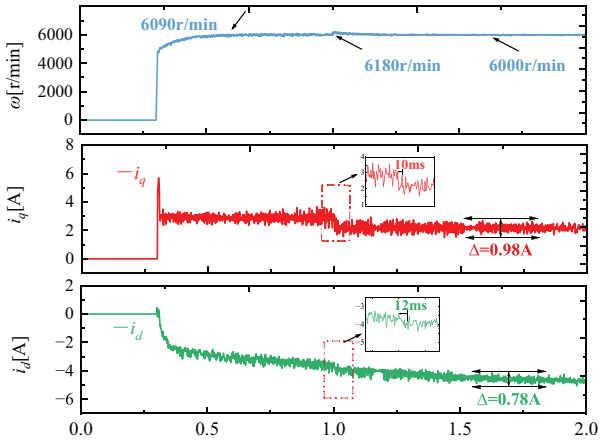

FIGURE 9. Conventional DPCC with load step disturbance.

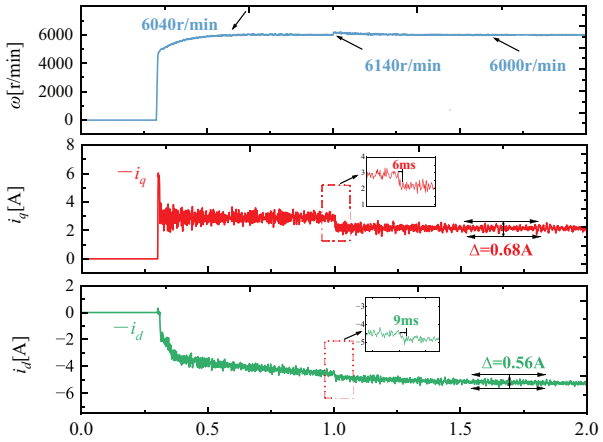

FIGURE 10. Proposed DPCC-PDSM with load step disturbance.

rated speed of the tested PMSM, the load was decreased from 0.6 N·m to 0.3 N·m, and an additional step disturbance of 0.4 N·m was applied at 1 s, resulting in a total load of 0.7 N·m at that instant. The controller sampling period was set to 10 μs (equivalent to 100 kHz). As shown in Fig. 8, the PI control method exhibited a pronounced overshoot, with the maximum speed reaching 6312 r/min. At 1 s, the speed stabilized at approximately 6200 r/min, which is 200 r/min higher than the steady-state reference. Meanwhile, the dynamic response of the currents was relatively slow, with the settling times of i_q and i_d being 12 ms and 16 ms, respectively. The current oscillation amplitudes reached $\Delta i_q = 1.06$ A and $\Delta i_d = 1.29$ A. These results indicate that the conventional PI controller in the flux weakening region suffers from significant dynamic lag and steady-state deviation under load disturbance and dead-time effects, reflecting its limited robustness.

In contrast, as illustrated in Figs. 9 and 10, the predictive control strategies achieved notable performance improvements. The conventional DPCC method reduced the overshoot to 6090 r/min, and the speed at 1 s reached 6180 r/min, corresponding to a deviation of 180 r/min. The settling times of i_q

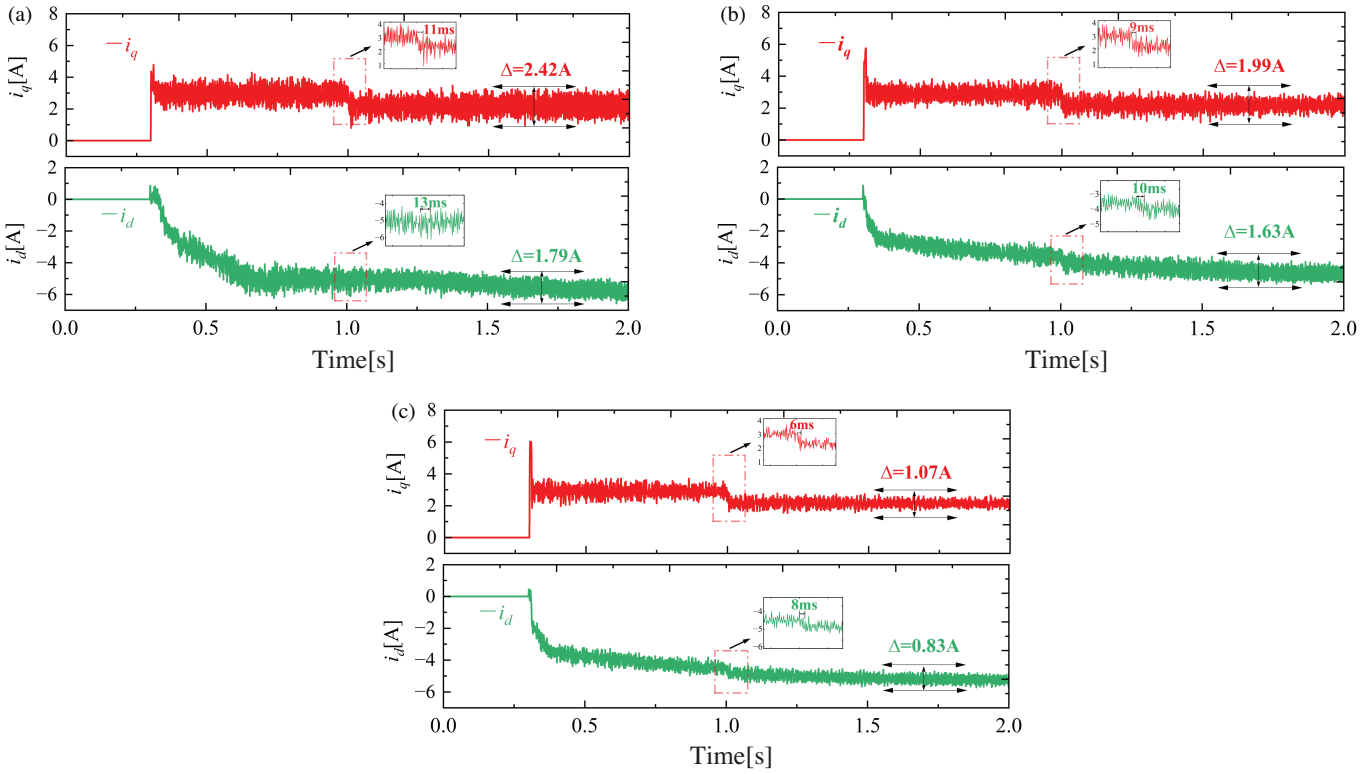

FIGURE 11. Current responses under a sudden 30 V perturbation on the u_α axis for the three control methods. For each subfigure, the top trace shows the q-axis current i_q, and the bottom trace shows the d-axis current i_d, with the corresponding deviations and transient response times indicated. (a) PI method. (b) Conventional DPCC method. (c) Proposed DPCC-PDSM method.

and i_d were shortened to 10 ms and 12 ms, while the current oscillation amplitudes decreased to 0.98 A and 0.78 A.

Furthermore, the proposed DPCC-PDSM method demonstrated superior dynamic behavior: the speed overshoot was further suppressed to 6040 r/min, and the speed at 1 s stabilized at approximately 6140 r/min, reducing the deviation to 140 r/min. The settling times of i_q and i_d were improved to 6 ms and 9 ms, indicating a 40–45% faster response than conventional DPCC. The current oscillation amplitudes were minimized to 0.68 A and 0.56 A, representing reductions of 35.8% and 56.6% compared with PI.

Overall, these comparative results clearly demonstrate that the DPCC-PDSM method provides significantly enhanced robustness and dynamic performance in the flux weakening region, effectively reducing overshoot, accelerating current transient response, and suppressing oscillations, thereby demonstrating superior engineering applicability compared with PI and conventional DPCC.

A voltage disturbance experiment was conducted, in which a sudden 30 V perturbation was injected into the u_α axis to evaluate the disturbance rejection performance of the three control strategies. As shown in Fig. 11(a), under PI control the deviations of i_q and i_d were 2.42 A and 1.79 A, respectively, indicating large current fluctuations and poor stability. As illustrated in Fig. 11(b), with the conventional DPCC method the deviations were reduced to 1.99 A and 1.63 A, demonstrating an improvement in disturbance suppression but still with considerable oscillations. Finally, as shown in Fig. 11(c), the proposed DPCC-PDSM method further decreased the deviations to 1.07 A and 0.83 A, corresponding to reductions about 55.8% and 53.6% compared with PI. These results clearly confirm that DPCC-PDSM significantly enhances current stability and robustness under sudden voltage disturbances.

5. CONCLUSION

In this article, a deadbeat predictive current control strategy based on a predictive disturbance suppression model, DPCC-PDSM, is proposed to enhance PMSM robustness. The main contributions can be summarized as follows:

A predictive disturbance suppression model is developed by integrating the recursive least squares algorithm with an ESO. This framework enables predictive compensation of current errors, ensuring effective disturbance rejection with low computational burden.

DPCC-PDSM is systematically evaluated against PI and conventional DPCC under sudden voltage perturbations and abrupt load torque steps. Results show that PI suffers from significant overshoot and oscillations, while DPCC achieves moderate improvement. In contrast, DPCC-PDSM suppresses the speed overshoot and reduces the steady-state speed deviation, which is about 22% lower than conventional DPCC. It also shortens the current settling times, corresponding to a 40–45% faster response. The current oscillation amplitudes are reduced, representing reductions of 35.8% and 56.6% compared with PI. In addition, under a sudden voltage perturbation, DPCC-PDSM

reduced the current deviations, corresponding to about 55% lower than PI.

The proposed method maintains current stability and dynamic tracking in high-speed flux weakening operation. Its ability to suppress both voltage disturbances and load variations highlights its practical value for high-performance PMSM drives.

Overall, the experimental results quantitatively confirm that DPCC-PDSM demonstrates excellent robustness, effectively reducing oscillations and overshoot while ensuring stable and reliable dynamic behavior under disturbances, thereby making it highly suitable for industrial PMSM drive applications.

ACKNOWLEDGEMENT

This work was supported by the Natural Science Foundation of the Jiangsu Higher Education Institution of China (24KJB470011).

REFERENCES

[1] Chen, Y., C. Liu, S. Liu, and Z. Song, "A new cascaded adaptive deadbeat control method for PMSM drive," *IEEE Transactions on Industrial Electronics*, Vol. 70, No. 4, 3384–3393, 2023.

[2] Wang, Y., S. Fang, and D. Huang, "An improved model-free active disturbance rejection deadbeat predictive current control method of PMSM based on data-driven," *IEEE Transactions on Power Electronics*, Vol. 38, No. 8, 9606–9616, 2023.

[3] Lin, X., W. Huang, W. Jiang, Y. Zhao, and S. Zhu, "Deadbeat direct torque and flux control for permanent magnet synchronous motor based on stator flux oriented," *IEEE Transactions on Power Electronics*, Vol. 35, No. 5, 5078–5092, 2020.

[4] Wang, F., D. Ke, X. Yu, and D. Huang, "Enhanced predictive model based deadbeat control for PMSM drives using exponential extended state observer," *IEEE Transactions on Industrial Electronics*, Vol. 69, No. 3, 2357–2369, 2022.

[5] Wu, C., Y. Zhao, and M. Sun, "Enhancing low-speed sensorless control of PMSM using phase voltage measurements and online multiple parameter identification," *IEEE Transactions on Power Electronics*, Vol. 35, No. 10, 10 700–10 710, 2020.

[6] Rovere, L., A. Formentini, and P. Zanchetta, "FPGA implementation of a novel oversampling deadbeat controller for PMSM drives," *IEEE Transactions on Industrial Electronics*, Vol. 66, No. 5, 3731–3741, 2019.

[7] Saeed, M. S. R., W. Song, B. Yu, and X. Feng, "Generalized deadbeat solution for model predictive control of five-phase PMSM drives," *IEEE Transactions on Power Electronics*, Vol. 38, No. 4, 5178–5191, 2023.

[8] Yan, H., W. Wang, Y. Xu, and J. Zou, "Position sensorless control for PMSM drives with single current sensor," *IEEE Transactions on Industrial Electronics*, Vol. 70, No. 1, 178–188, 2023.

[9] Zhang, X. and Y. Cao, "A simple deadbeat predictive current control for PMSM with parameter robustness improvement," *IEEE Journal of Emerging and Selected Topics in Power Electronics*, Vol. 13, No. 1, 759–770, 2025.

[10] Song, W., J. Li, C. Ma, Y. Xia, and B. Yu, "A simple tuning method of PI regulators in FOC for PMSM drives based on deadbeat predictive conception," *IEEE Transactions on Transportation Electrification*, Vol. 10, No. 4, 9852–9863, 2024.

[11] Wang, L., S. Zhang, C. Zhang, and Y. Zhou, "An improved deadbeat predictive current control based on parameter identification for PMSM," *IEEE Transactions on Transportation Electrification*, Vol. 10, No. 2, 2740–2753, 2024.

[12] Wang, H., C. Gan, H. Ren, C. Zhang, X. Shan, and R. Qu, "An input-delay compensation strategy for deadbeat predictive current control of PMSM," *IEEE Transactions on Industrial Electronics*, 2025.

[13] Zhou, Z. and S. Yao, "Deadbeat direct current control using dynamic time programming for six-phase PMSM drives with open-phase faults," *IEEE Transactions on Industrial Electronics*, Vol. 71, No. 9, 10 064–10 074, 2024.

[14] Li, R., D. Huang, Y. Chen, and Q. Zhao, "Deadbeat predictive speed control of PMSM via enhanced low-gain disturbance observer design and inertia identification," *IEEE Journal of Emerging and Selected Topics in Power Electronics*, Vol. 13, No. 2, 2524–2534, 2025.

[15] Lei, J., S. Fang, D. Huang, and Y. Wang, "Enhanced deadbeat predictive current control for PMSM drives using iterative sliding mode observer," *IEEE Transactions on Power Electronics*, Vol. 38, No. 11, 13 866–13 876, 2023.

[16] Wu, X., H. Chen, B. Liu, T. Wu, C. Wang, and S. Huang, "Improved deadbeat predictive current control of PMSM based on a resistance adaptive position observer," *IEEE Transactions on Transportation Electrification*, Vol. 10, No. 3, 5215–5224, 2024.

[17] Cao, H., Y. Deng, J. Liu, Y. Zuo, X. Liu, H. Wang, and C. H. T. Lee, "Improved deadbeat predictive current control of PMSM drives with repetitive control-based disturbance correction observer," *IEEE Transactions on Power Electronics*, Vol. 40, No. 1, 801–812, 2025.

[18] Wang, W., C. Liu, H. Zhao, and Z. Song, "Improved deadbeat-direct torque and flux control for PMSM with less computation and enhanced robustness," *IEEE Transactions on Industrial Electronics*, Vol. 70, No. 3, 2254–2263, 2023.

[19] Li, X., Y. Yang, J. Sun, Y. Xiao, M. Fan, K. Ni, J. Hu, H. Wen, H. Yang, and J. Rodriguez, "Multiple-voltage-vector model-free predictive deadbeat control with updated reference voltage vector for PMSM drive," *IEEE Transactions on Power Electronics*, Vol. 40, No. 5, 6492–6505, 2025.

[20] Zhang, X., Z. Wang, and H. Bai, "Sliding-mode-based deadbeat predictive current control for PMSM drives," *IEEE Journal of Emerging and Selected Topics in Power Electronics*, Vol. 11, No. 1, 962–969, 2023.

[21] Tian, M., B. Wang, Y. Yu, Q. Dong, and D. Xu, "Static-errorless deadbeat predictive current control for PMSM current harmonics suppression based on vector resonant controller," *IEEE Transactions on Power Electronics*, Vol. 38, No. 4, 4585–4595, 2023.

[22] Miguel-Espinar, C., D. Heredero-Peris, G. Gross, M. Llonch-Masachs, and D. Montesinos-Miracle, "Maximum torque per voltage flux-weakening strategy with speed limiter for PMSM drives," *IEEE Transactions on Industrial Electronics*, Vol. 68, No. 10, 9254–9264, 2021.

[23] Liu, S., C. Liu, H. Zhao, Y. Liu, and Z. Dong, "Improved flux weakening control strategy for five-phase PMSM considering harmonic voltage vectors," *IEEE Transactions on Power Electronics*, Vol. 37, No. 9, 10 967–10 980, 2022.

[24] Zhao, W., L. Li, B. Wang, G. Zhu, N. Wang, and X. Wang, "Improved leading-angle flux-weakening control for surface-inset permanent magnet synchronous motor considering asymmetric rotor effects," *IEEE Transactions on Power Electronics*, Vol. 40, No. 7, 9699–9708, 2025.

[25] Shuaib Akbar, K. T. and P. K. Abraham, "Variable load torque performance analysis in flux weakening control of PMSM," in *2022 IEEE 19th India Council International Conference (INDICON)*, 1–5, Kochi, India, 2022.

[26] Zhang, X., Z. Zhao, and C. Xu, "A flux-weakening method for PMSM based model predictive direct speed control," in *2020 IEEE 9th International Power Electronics and Motion Control Conference (IPEMC2020-ECCE Asia)*, 2557–2561, Nanjing, China, 2020.

[27] Yoo, J., J. Lee, and S.-K. Sul, "Analysis of instability in torque control of sensorless PMSM drives in flux weakening region," *IEEE Transactions on Power Electronics*, Vol. 36, No. 9, 10 815–10 826, 2021.

[28] Wang, L., Y. Yu, B. Wang, and D. Xu, "Bandwidth-based tuning method for PMSM field-weakening control with speed adaptation," *IEEE Transactions on Industrial Electronics*, 2025.

[29] Zhao, W., N. Wang, B. Wang, G. Zhu, D. Chen, and X. Wang, "Flux weakening control strategy for asymmetric surface inset permanent magnet synchronous motors based on reoriented dq-axis reference frame," *IEEE Transactions on Industrial Electronics*, Vol. 72, No. 6, 5658–5668, 2025.

[30] Hu, Y., Y. Li, X. Ma, X. Li, and S. Huang, "Flux-weakening control of dual three-phase PMSM based on vector space decomposition control," *IEEE Transactions on Power Electronics*, Vol. 36, No. 7, 8428–8438, 2021.

[31] Navarro-Temoche, A., J. Jugo, E. Ibarra, and I. Kortabarria, "Model predictive flux weakening controller for asymmetrical dual three-phase PMSM drives," in *2025 IEEE Workshop on Electrical Machines Design, Control and Diagnosis (WEMDCD)*, 1–6, Valletta, Malta, 2025.

[32] Zhang, X., B. Wang, Y. Yu, J. Zhang, and D. Xu, "Torque adaptive hexagon voltage extension method for PMSM flux-weakening control based on dual PI cascade structure," *IEEE Transactions on Power Electronics*, Vol. 38, No. 1, 332–345, 2022.